Photoacoustic tomography: a potential new tool for prostate cancer

Xueding Wang,[1,*] William W. Roberts,[2] Paul L. Carson,[1] David P. Wood,[2] and J. Brian Fowlkes[1]

[1]*Department of Radiology, University of Michigan School of Medicine, Ann Arbor, MI 48109, USA*
[2]*Department of Urology, University of Michigan School of Medicine, Ann Arbor, MI 48109, USA*
**xdwang@umich.edu*

Abstract: The feasibility of photoacoustic tomography (PAT) for noninvasive imaging of prostate cancer was explored through the study on a canine model *in vivo*. Imaging of blood-rich lesions mimicking prostate tumors was achieved using a commercial medical ultrasound (US) system without affecting its original imaging functions. Based on the optical contrast between hemoglobin and other tissues, PAT has demonstrated good sensitivity and high contrast-to-noise ratio in visualizing deep lesions; while US has presented the morphological features including the boundary and the urethral of the prostate. PAT of prostate cancer may facilitate improved tumor localization, staging of disease, and detection of recurrences.

OCIS codes: (170.5120) Photoacoustic imaging; (170.3880) Medical and biological imaging; (170.0110) Imaging systems.

References and links

1. American Cancer Society, *Cancer facts and Figs. 2010*. Atlanta: American Cancer Society; 2010.
2. M. L. Lefevre, "Prostate cancer screening: more harm than good?" Am. Fam. Physician **58**(2), 432–438 (1998).
3. M. Norberg, L. Egevad, L. Holmberg, P. Sparén, B. J. Norlén, and C. Busch, "The sextant protocol for ultrasound-guided core biopsies of the prostate underestimates the presence of cancer," Urology **50**(4), 562–566 (1997).
4. H. Wijkstra, M. H. Wink, and J. J. de la Rosette, "Contrast specific imaging in the detection and localization of prostate cancer," World J. Urol. **22**(5), 346–350 (2004).
5. R. Ross, and M. Harisinghani, "New clinical imaging modalities in prostate cancer," Hematol. Oncol. Clin. North Am. **20**(4), 811–830 (2006).
6. B. Turkbey, P. A. Pinto, P. L. Choyke; Medscape, "Imaging techniques for prostate cancer: implications for focal therapy," Nat. Rev. Urol. **6**(4), 191–203 (2009).
7. T. C. Potdevin, A. P. Moskalik, J. B. Fowlkes, R. O. Bude, and P. L. Carson, "Doppler quantitative measures by region to discriminate prostate cancer," Ultrasound Med. Biol. **27**(10), 1305–1310 (2001).
8. M. J. Mitterberger, F. Aigner, W. Horninger, H. Ulmer, S. Cavuto, E. J. Halpern, and F. Frauscher, "Comparative efficiency of contrast-enhanced colour Doppler ultrasound targeted versus systematic biopsy for prostate cancer detection," Eur. Radiol. (2010).
9. H. Hricak, P. L. Choyke, S. C. Eberhardt, S. A. Leibel, and P. T. Scardino, "Imaging prostate cancer: a multidisciplinary perspective," Radiology **243**(1), 28–53 (2007).
10. J. H. Ali, W. B. Wang, M. Zevallos, and R. R. Alfano, "Near infrared spectroscopy and imaging to probe differences in water content in normal and cancer human prostate tissues," Technol. Cancer Res. Treat. **3**(5), 491–497 (2004).
11. S. A. Boppart, J. M. Herrmann, C. Pitris, D. L. Stamper, M. E. Brezinski, and J. G. Fujimoto, "Real-time optical coherence tomography for minimally invasive imaging of prostate ablation," Comput. Aided Surg. **6**(2), 94–103 (2001).
12. A. V. D'Amico, M. Weinstein, X. Li, J. P. Richie, and J. Fujimoto, "Optical coherence tomography as a method for identifying benign and malignant microscopic structures in the prostate gland," Urology **55**(5), 783–787 (2000).
13. G. Xu, D. Piao, C. H. Musgrove, C. F. Bunting, and H. Dehghani, "Trans-rectal ultrasound-coupled near-infrared optical tomography of the prostate, part I: simulation," Opt. Express **16**(22), 17484–17504 (2008).
14. Z. Jiang, D. Piao, G. Xu, J. W. Ritchey, G. R. Holyoak, K. E. Bartels, C. F. Bunting, G. Slobodov, and J. S. Krasinski, "Trans-rectal ultrasound-coupled near-infrared optical tomography of the prostate, part II: experimental demonstration," Opt. Express **16**(22), 17505–17520 (2008).
15. G. Ku, X. Wang, X. Xie, G. Stoica, and L. V. Wang, "Imaging of tumor angiogenesis in rat brains in vivo by photoacoustic tomography," Appl. Opt. **44**(5), 770–775 (2005).

#135176 - $15.00 USD Received 15 Sep 2010; revised 1 Oct 2010; accepted 5 Oct 2010; published 7 Oct 2010

16. X. Wang, X. Xie, G. Ku, L. V. Wang, and G. Stoica, "Noninvasive imaging of hemoglobin concentration and oxygenation in the rat brain using high-resolution photoacoustic tomography," J. Biomed. Opt. **11**(2), 024015 (2006).
17. H. F. Zhang, K. Maslov, G. Stoica, and L. V. Wang, "Functional photoacoustic microscopy for high-resolution and noninvasive in vivo imaging," Nat. Biotechnol. **24**(7), 848–851 (2006).
18. R. G. M. Kolkman, P. J. Brands, W. Steenbergen, and T. G. van Leeuwen, "Real-time in vivo photoacoustic and ultrasound imaging," J. Biomed. Opt. **13**(5), 050510 (2008).
19. T. N. Erpelding, C. Kim, M. Pramanik, L. Jankovic, K. Maslov, Z. J. Guo, J. A. Margenthaler, M. D. Pashley, and L. V. Wang, "Sentinel lymph nodes in the rat: noninvasive photoacoustic and US imaging with a clinical US system," Radiology **256**(1), 102–110 (2010).
20. M. A. Yaseen, S. A. Ermilov, H. P. Brecht, R. Su, A. Conjusteau, M. Fronheiser, B. A. Bell, M. Motamedi, and A. A. Oraevsky, "Optoacoustic imaging of the prostate: development toward image-guided biopsy," J. Biomed. Opt. **15**(2), 021310 (2010).
21. X. Wang, J. B. Fowkes, P. L. Carson, and L. Mo, "Experimental Evaluation of a High-Speed Photoacoustic Tomography System based on a Commercial Ultrasound Unit," in 2008 Proc.-IEEE Ultrason. Symp. Vols 1–4 and Appendix (2008), pp. 1234–1237.
22. C. Kim, T. N. Erpelding, K. Maslov, L. Jankovic, W. J. Akers, L. Song, S. Achilefu, J. A. Margenthaler, M. D. Pashley, and L. V. Wang, "Handheld array-based photoacoustic probe for guiding needle biopsy of sentinel lymph nodes," J. Biomed. Opt. **15**(4), 046010 (2010).
23. American National Standards Institute, American national standard for the safe use of lasers. Standard Z136.1–2007, ANSI, Inc., New York, NY (2007).
24. M. Xu, and L. V. Wang, "Analytic explanation of spatial resolution related to bandwidth and detector aperture size in thermoacoustic or photoacoustic reconstruction," Phys. Rev. E Stat. Nonlin. Soft Matter Phys. **67**(5), 056605 (2003).
25. Y. Xu, L. V. Wang, G. Ambartsoumian, and P. Kuchment, "Reconstructions in limited-view thermoacoustic tomography," Med. Phys. **31**(4), 724–733 (2004).
26. D. W. Yang, D. Xing, S. H. Yang, and L. Z. Xiang, "Fast full-view photoacoustic imaging by combined scanning with a linear transducer array," Opt. Express **15**(23), 15566–15575 (2007).
27. C. Zhang, and Y. Wang, "Deconvolution reconstruction of full-view and limited-view photoacoustic tomography: a simulation study," J. Opt. Soc. Am. A **25**(10), 2436–2443 (2008).
28. C. Tao, and X. J. Liu, "Reconstruction of high quality photoacoustic tomography with a limited-view scanning," Opt. Express **18**(3), 2760–2766 (2010).
29. X. Wang, Y. Pang, G. Ku, X. Xie, G. Stoica, and L. V. Wang, "Noninvasive laser-induced photoacoustic tomography for structural and functional in vivo imaging of the brain," Nat. Biotechnol. **21**(7), 803–806 (2003).
30. X. Wang, Y. Pang, G. Ku, G. Stoica, and L. V. Wang, "Three-dimensional laser-induced photoacoustic tomography of mouse brain with the skin and skull intact," Opt. Lett. **28**(19), 1739–1741 (2003).
31. M. A. Yaseen, S. A. Ermilov, H. P. Brecht, R. Su, A. Conjusteau, M. Fronheiser, B. A. Bell, M. Motamedi, and A. A. Oraevsky, "Optoacoustic imaging of the prostate: development toward image-guided biopsy," J. Biomed. Opt. **15**(2), 021310 (2010).

1. Introduction

In North America, prostate cancer is the most common noncutaneous malignancy affecting men and has the highest mortality rate after lung cancer [1]. Current screening techniques, including digital rectal examination (DRE) and the measurement of prostate specific antigen (PSA) levels in the blood, do not adequately provide the information needed to make treatment decisions [2]. Diagnosis of prostate cancer remains dependent upon histologic assessment of cancer from tissue biopsies. Ultrasonography of the prostate remains the first choice of imaging to visualize the prostate. However, gray-scale ultrasound imaging has an accuracy of about 50-60% for the detection of prostate cancer and transrectal ultrasound (TRUS) used for local grading has an even lower accuracy [3–5]. Because other disease processes such as benign prostatic hyperplasia (BPH) and prostatitis may have a similar appearance to prostate cancer, it is difficult to reliably differentiate these lesions from prostate cancer based on sonographic characteristics alone. Despite the recent development in sonographic vascular imaging (e.g. color and power Doppler, and introduction of ultrasound contrast agents), TRUS is still confined to the guidance of prostate biopsy. Although TRUS by itself has limited sensitivity and specificity in the detection of prostate cancer, TRUS images combined with other types of imaging data could improve tumor localization, staging of disease, and detection of recurrences [6]. The modest success of color Doppler and contrast enhanced ultrasound [7,8] suggest that the improved detection by PAT of tissue blood volume and state of oxygenation, discussed below, could yield unique clinical utility of PAT.

Adaptation of novel optical modalities to cancer imaging is highly desirable because nonionizing optical signal is sensitive to the molecular conformation of biological tissues and

#135176 - $15.00 USD Received 15 Sep 2010; revised 1 Oct 2010; accepted 5 Oct 2010; published 7 Oct 2010

is closely related to physiological states such as blood oxygenation and blood volume. With unique advantages, optical imaging should contribute to more accurate characterization of prostate cancer through the synthesis of anatomic, functional, and molecular imaging information [9]. It has been reported that near-infrared spectroscopy (NIRS) can been used to differentiate cancerous tissues and normal tissues in prostates based on their different spectral fingerprint absorption [10]. Optical coherence tomography (OCT) has also been adapted to prostate cancer and has demonstrated potential in monitoring the dynamic process of laser and radiofrequency ablation [11] and in identifying benign and malignant microscopic structures in the prostate gland [12]. More recently, the feasibility of transrectal optical tomography of the prostate using an endorectal near-infrared (NIR) applicator integrated with a TRUS probe has been investigated [13,14]. Diffuse optical imaging of prostate, however, has only limited resolution because of the strong photon diffusion in biological tissues, which drastically hinders the clinical application of optical imaging in prostate cancer detection and evaluation. OCT, although delivering excellent spatial resolution, has only limited penetration in biological tissue and, hence, cannot evaluate a prostate noninvasively as a whole organ.

Photoacoustic tomography (PAT), also referred to as optoacoustic tomography, is an emerging hybrid imaging modality that is noninvasive, nonionizing, with high sensitivity, satisfactory imaging depth for the prostate and good temporal and spatial resolution. PAT is a natural complement to existing ultrasonography and should enlarge the scope of US in diagnostic imaging and therapeutic monitoring of prostate cancer by providing additional information. Numerous previous studies have demonstrated that new blood vessel growth, termed angiogenesis, is essential for growth and metastasis of most solid tumors including prostate cancer. PAT, based on its high sensitivity to blood, may evaluate tumor-related vascular distortion, including both angiogenesis and dilation of blood vessels in cancerous tissues [15]. The increased blood volume in tumor regions, a functional hallmark of prostate cancer, might be detected and localized reliably by PAT with high optical contrast and high spatial resolution. When working with multiple laser wavelengths, PAT may also quantify the inadequate oxygen delivery, i.e. profound hypoxia and oxidative stress, in local tumors as another functional hallmark of prostate cancer [16,17]. When PAT is realized based on a commercial US unit [18–22], the dual-modality imaging capability will allow inexpensive, nonionizing and noninvasive visualization of both acoustic and optical tissue properties as well as physiological biomarkers of prostate cancer including blood flow by Doppler US and blood volume and oxygenation by PAT. With the comprehensive diagnostic information presented by a combined US and PAT prostate imaging system, more accurate characterization of prostate cancer could be achieved than by using conventional transrectal US alone.

2. Method

A high-speed PAT data acquisition system was assembled using a commercial US scanner working with a P4-1 phased array (z.one, ZONARE Medical Systems, Inc.), as shown in Fig. 1. A Nd:YAG laser (Powerlite, Continuum) pumped dye laser (ND6000, Continuum) provides laser pulses with a repetition rate of 10 Hz, wavelength of 710 nm, and a pulse length of 5 ns. The laser-generated photoacoustic signals are acquired by the US unit; synchronization between the US receive cycle and the laser firing is achieved using a frame-trigger signal tapped into the ultrasonic probe connector. To acquire a 2D PAT image in a prostate, the US unit operates in receive-only mode (with the transmitter turned off) at a frame rate that matches the 10 Hz repetition rate of the laser; while working on the US mode with the transmitter turned on, B-mode US images of the same imaging plane in the prostate can be taken. For command and control, a serial (RS-232) data link is set up between the US unit and an external PC. Through a Tera Term console that supports serial communications between the US unit and the PC, the user runs a command script that sends imaging control parameters to the US unit, including the start of data acquisition, transmitter on/off, transmit delays, acquisition frame rate, time-gain compensation, and demodulation frequency.

#135176 - $15.00 USD Received 15 Sep 2010; revised 1 Oct 2010; accepted 5 Oct 2010; published 7 Oct 2010

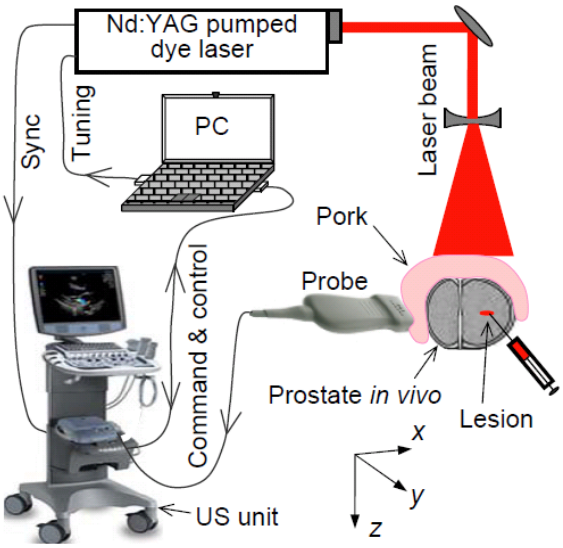

Fig. 1. Schematic of the experimental system for PAT and US imaging of a canine prostate *in vivo*.

For each laser pulse, 64 channels of 16-bit in-phase quadrature (I/Q) data are acquired from a selectable 64-element sub-aperture of the array. Therefore, only 2 laser pulses are required for the acquisition of a complete 128-element data set for a 2D PAT image, at an effective full frame rate acquisition of 5 Hz. If needed, repeat acquisitions are made to support coherent data averaging for improved signal-to-noise ratios (SNR). Once the I/Q data including both reconstructed and channel data are captured in the cine buffer, they can be transferred as binary raw data files to an external USB storage device. On the PC, a MATLAB tool is used to extract the raw I/Q data and associated imaging parameters from binary data files. The RF data from the 64 or 128 elements are then processed using a standard ultrasound dynamic receive focusing algorithm to reconstruct a PAT image.

Before the experiment on canine prostates *in vivo*, the lateral and axial resolution of this PAT system were evaluated by imaging a micro-flow vessel phantom made from a transparent soft tube (I.D. 0.5 mm, Cole-Parmer) filled with fresh canine blood. With the orientation of the vessel orthogonal to the transducer array, a point object was formed in the 2D B-scan plane when the vessel was illuminated by a narrow laser beam. The delay curve in Fig. 2(A) shows the I/Q data of received photoacoustic signals from the point object acquired by the 128 array elements. This signal was induced by a single laser pulse with an incident energy density within the ANSI safety limit [23]. The fast Fourier transform (FFT) of the RF data converted from the I/Q data indicated that the imaging system working with the P4-1 array was sensitive in the spectrum of 1.5-4.2 MHz with a fairly broad –6 dB receiving bandwidth of 94%. Using the standard ultrasound dynamic receive focusing algorithm, a 2D PAT image of the point object was reconstructed, as shown in Fig. 2(B). By studying the image intensities through the center of the point object along the axial (depth) and the lateral (azimuthal) directions [as shown in Figs. 2(C) and 2(D) respectively], the –6 dB axial and lateral resolution achieved by this system were 0.65 mm and 0.52 mm, respectively, at a depth of 20 mm where the azimuthal f-number was approximately 0.7.

#135176 - $15.00 USD Received 15 Sep 2010; revised 1 Oct 2010; accepted 5 Oct 2010; published 7 Oct 2010

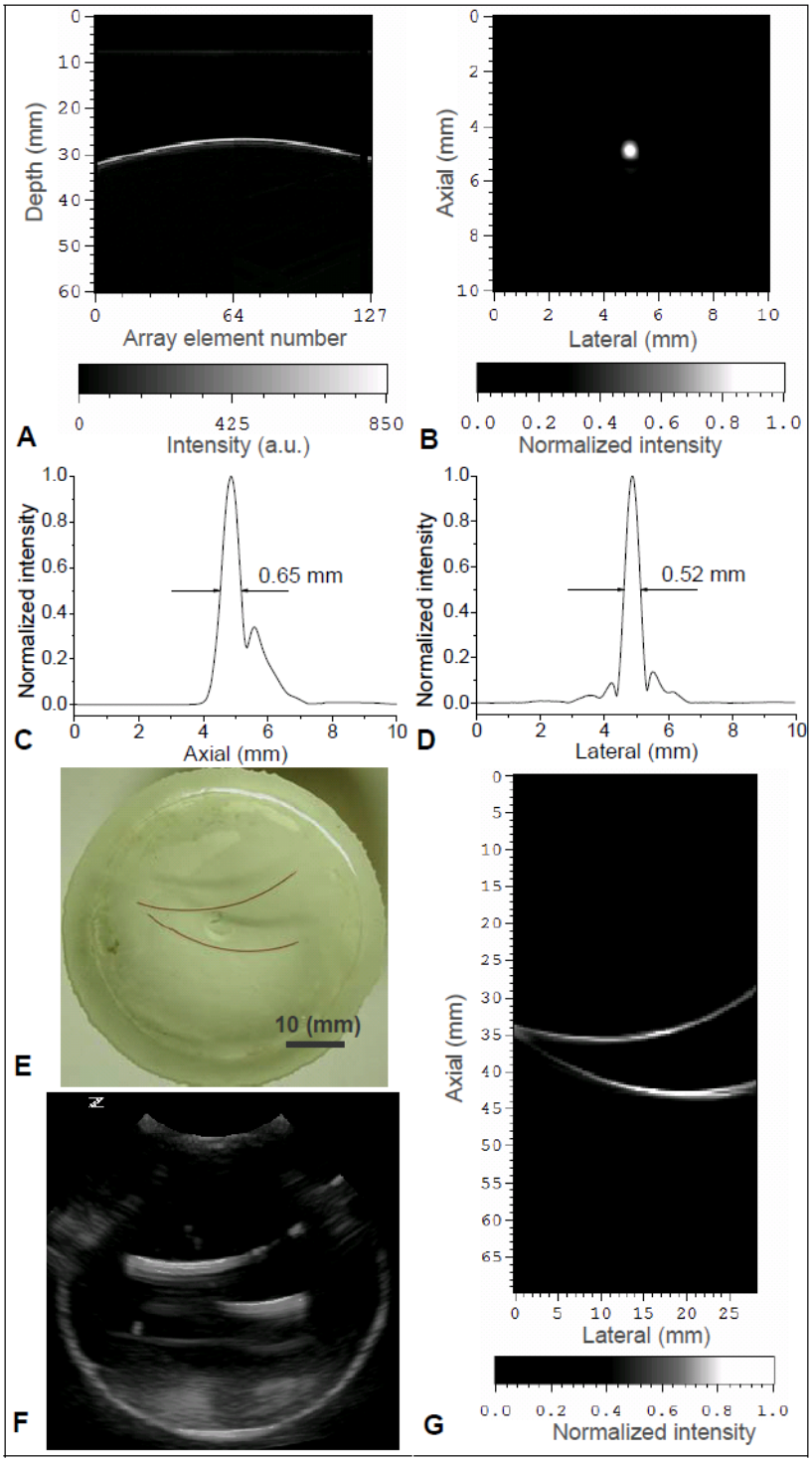

Fig. 2. (A) 128-channel I/Q data from a point object. (B) Reconstructed 2D PAT image of the point object. (C) System axial resolution. (D) System lateral resolution. (E) Photograph of a gel phantom with two artificial vessels embedded. (F) 2D gray scale US image of the phantom (G) 2D PAT image of the phantom along the same plane as in US image in (F).

#135176 - $15.00 USD Received 15 Sep 2010; revised 1 Oct 2010; accepted 5 Oct 2010; published 7 Oct 2010

In order to examine the capability of this system in mapping highly absorbing vasculature, a micro-flow vessel phantom with known vascular structure was imaged. As shown in Fig. 2(E), two vessels made with the same transparent soft tubing (I.D. 0.5 mm) as above, filled with fresh canine blood, were embedded in the same 2D plane in a block of porcine gel. First, a 2D gray scale pulse echo US image of this phantom was taken, as shown in Fig. 2(F). The apparent poor axial resolution is caused by reverberations in the tube. Then without moving the sample or the probe, the system shifted to PAT mode with the US transmitter turned off. When illuminated by laser light at 850-nm wavelength with incident light fluence within the ANSI safety limit, a PAT image of the same 2D cross-section was taken, as shown in Fig. 2(G). The B-scan PAT image was reconstructed using the signals from the full 128 elements without apodization. Based on the strong optical absorption contrast between the canine blood and the background gel, the two vessels were imaged with satisfactory continuity, resulting in a good match with the sample photograph.

3. Animal model

To examine the performance of this system for PAT and US dual-modality imaging of prostate, scanning of canine prostates *in vivo* was conducted. The laboratory animal protocol for this work was approved by the UCUCA of the University of Michigan. All dogs were pre-anesthitized by an IM injection of Acepromazine, administered thiopental to effect for anesthesia induction, intubated, and full anesthesia maintained by inhalation of Isoflurane. The animal was instrumented with a pulse-oximeter to measure pulse and SPO_2, ECG, core body temperature and respiration during the entire experiment. The suprapubic area of all animals was shaved. Entry to the abdomen was through a lower midline vertical incision approximately 30 cm in length. The bladder was identified, atraumatically mobilized and retracted cephalad to facilitate exposure of the underlying prostate.

To validate the feasibility of PAT for future noninvasive transrectal imaging of prostate cancer, this experiment focused on the ability of PAT, with incident NIR energy within the ANSI safety limit, to capture blood-rich lesions in subsurface prostate *in vivo* through reasonable optical and ultrasonic path lengths. To mimic the characteristics of tumor, pseudo lesions were induced by intraprostatic injection of varying amounts of fresh canine blood, in light of the increased angiogenic nature of prostate cancer lesions and thus relatively increased hemoglobin levels. Blood collected from the same dog was injected through a plastic canula inserted to the midline lateral surface of one lobe of the exposed prostate. 2D B-scan PAT and US imaging of a cross-section in the X-Y plane through the lesion were conducted. In order to guarantee that the lesion is within the imaged cross-section, gray scale US scan over the whole prostate was performed first to locate the end of the inserted canula. The laser beam, after being expanded and homogenized, illuminated along the Z-axis covering a round area with a diameter of 4 cm. With a total input energy of 100 mJ, the incident light energy density on the tissue was approximately 8 mJ/cm^2, well below the ANSI safety limit. In order to examine the ability of PAT to image deep prostate lesions through the rectal wall, a slab of fresh pork muscle (15 mm thick) was also used to cover the surface of the exposed prostate, mimicking the connective tissue between prostate and rectum. Therefore, since the depth of the lesion in the prostate was about 10 mm, the optical and ultrasound path lengths were both approximately 25 mm.

#135176 - $15.00 USD Received 15 Sep 2010; revised 1 Oct 2010; accepted 5 Oct 2010; published 7 Oct 2010

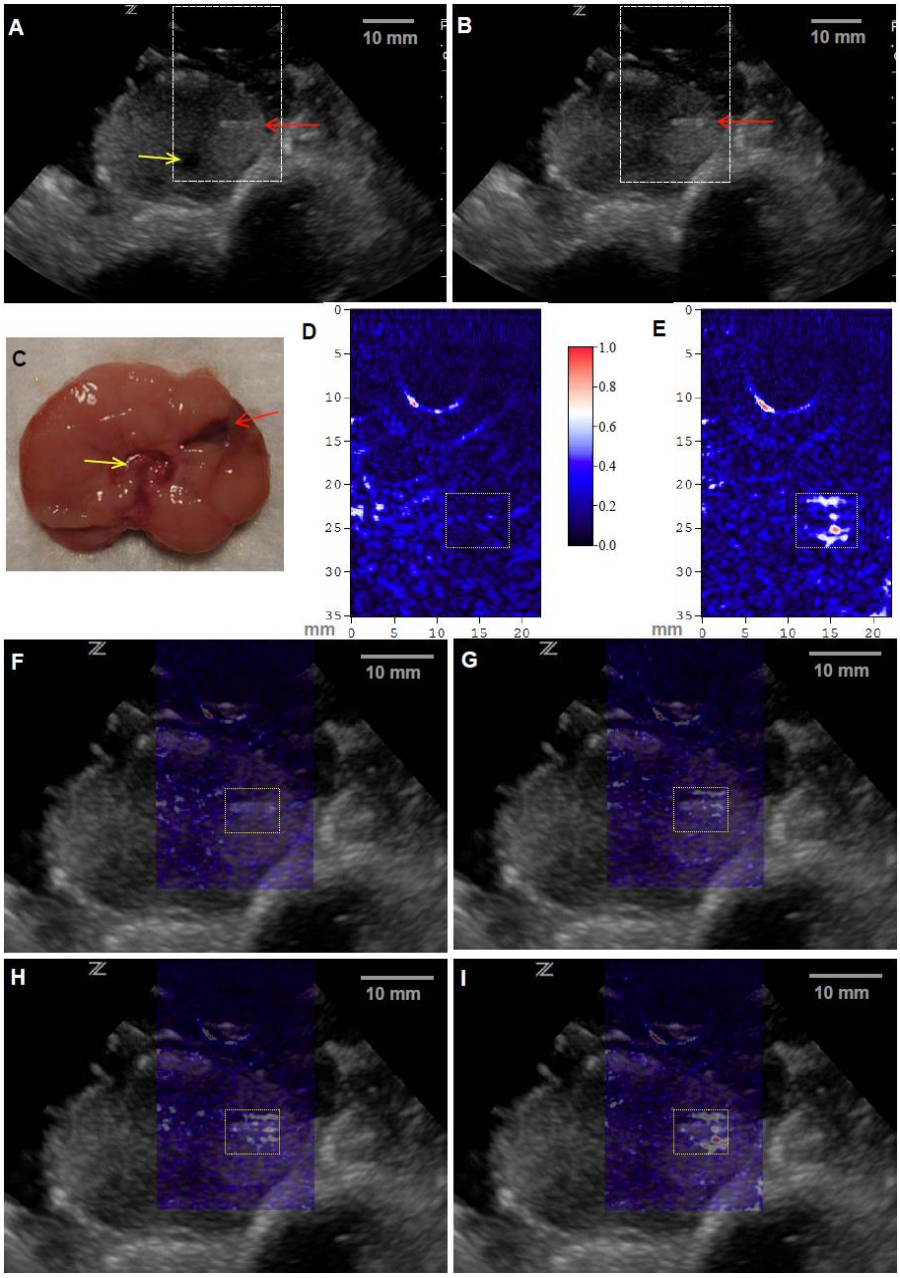

Fig. 3. *In vivo* PAT and US dual-modality imaging of a canine prostate with a subsurface lesion induced. Gray scale US images of the prostate acquired (A) before and (B) after the generation of the lesion (0.1 mL of injected blood). The red arrow indicates the plastic canula inserted into the prostate for the injection of blood. The yellow indicates the urethra. (C) Anatomical photograph of the imaged cross-section in the prostate with the lesion marked. PAT images of the prostate right lobe acquired (D) before and (E) after the generation of the lesion (0.1 mL of injected blood), where the image intensities are demonstrated with an image color bar. The PAT imaging plane is the same as that in US images, where the reconstructed area is indicated with the dashed rectangles in the US images in (A) and (B). In (F)-(I), PAT images are superimposed on the US image in (B). (F) was acquired before the generation of the lesion; (G), (H) and (I) were acquired after three injections of blood, where the total blood volumes in the lesion were 0.025 mL, 0.05 mL and 0.1 mL, respectively. The area of the lesion is marked with a dotted rectangle in each image.

#135176 - $15.00 USD Received 15 Sep 2010; revised 1 Oct 2010; accepted 5 Oct 2010; published 7 Oct 2010

4. Result

Before generation of the pseudo lesion, US and PAT images of the canine prostate were taken, as shown in Figs. 3(A) and 3(D). In the gray-scale B-mode US images, morphological features of the prostate including the boundary and the urethra (yellow arrow), as well as the plastic canula (red arrow) inserted into the prostate for the generation of the lesion, can be clearly recognized. During the experiment, three local injections of canine blood were performed through the plastic canula without moving the prostate or the US probe. The doses of the three injections were 0.025, 0.025 and 0.050 mL respectively. Therefore, the total additional blood volumes in the lesion area after the three injections were 0.025, 0.05 and 0.1 mL (i.e. 1:2:4). After each injection, US and PAT images of the same cross-section were taken. Comparing the two US images taken before and after the generation of the lesion, no obvious change can be noticed in the lesion area due to the limited contrast of US in imaging small volumes of static blood. Because of the high sensitivity of PAT for blood content, the signal enhancement in the lesion area in Fig. 3(E) (marked with a dotted rectangle) can be seen clearly in comparision with Fig. 3(D). In Fig. 3(F)–3(I), four PAT images taken before and after the three injections respectively are superimposed on the gray-scale US image in Fig. 3(B), where a color bar is given to present the PAT image intensity. With the morphological features presented by the US image, we can see that the signal enhancement in each PAT image is around the tip of the plastic canula, i.e. in the generated lesion. To quantitatively evaluate the signal enhancement as a function of the injected blood volume, we have computed the mean intensity for all the pixels in the dotted rectangle in each PAT image. The mean intensity values in the lesion area are 0.25, 0.35, 0.47 and 0.59 for the results in Figs. 3(F)–3(I) respectively. Therefore, the signal increases over no injections are 0.10, 0.22 and 0.34, respectively, after the three injections. The ratio among three increases are 1:2.2:3.4, close to the ratio among the total introduced blood volumes after the three injections (i.e. 1:2:4). The good match between the photoacoustic signal enhancement and the total injected blood volume of the lesion suggests that PAT, with its high optical contrast and good spatial resolution, may not only visualize local prostate lesions in a noninvasive manner but also characterize the functional parameters in lesions such as total hemoglobin concentration (i.e. blood volume).

5. Discussion

In PAT, the ability to achieve high depth of imaging is primarily a function of total laser pulse energy of short enough duration and illuminating the tissues over a large enough area to remain below the ANSI safety limit. For tomographic photoacoustic imaging of deep tissue, the ability to achieve high image quality including good spatial resolution and less artifacts is strongly dependent on the total view angle (or solid angle in 3D imaging) in detecting photoacoustic signals, even though some advanced reconstruction algorithms have been explored for improved performance in limited-viewing angle situations [24–28]. To study the effect of different detection view angle on the image quality, *ex vivo* imaging of a canine prostate was conducted through a circular scan of a single element transducer (V312, Panametrics). The geometry of signal detection from the prostate was similar to that developed for imaging of small animal brains [29,30]. Briefly, the cylindrically focused transducer (unfocused in the imaging plane) with a center frequency at 10 MHz and a –6 dB bandwidth of 130% collected signals from the prostate through a circular scan around the imaged cross-section, while the laser beam illuminated the whole prostate with an incident direction orthogonal to the imaging plane. To cover a 2π view angle, 160 points around the prostate were acquired at 2.25 degree increments. Figure 4(B) presents the 2D image reconstructed using the signals received from a full 2π angular range. Based on the intrinsic optical contrast among soft tissues, morphological features in the prostate, including the area of periurethral gland (i.e. the zone surrounding the urethra) and the gap between the left and right lobes, were imaged with satisfactory resolution and minimal artifacts. When the view angle for reconstructed signals was decreased, the artifact in the reconstructed image was

#135176 - $15.00 USD Received 15 Sep 2010; revised 1 Oct 2010; accepted 5 Oct 2010; published 7 Oct 2010

stronger and the lateral resolution also degraded, as demonstrated in Fig. 4(C)–4(F) where the detection view angles were 180, 90, 60 and 30 degrees, respectively.

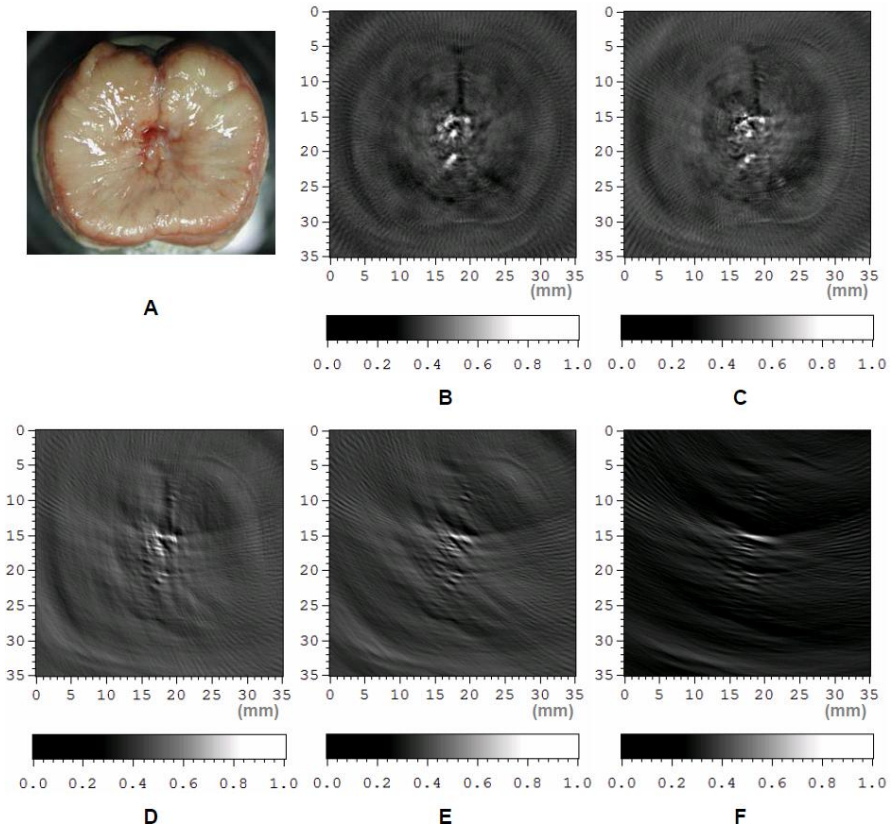

Fig. 4. *Ex vivo* 2D PAT of a canine prostate. (A) Anatomical photograph of the imaged cross-section. (B)-(F) Tomographic images acquired with detection view angles of 360, 180, 90, 60 and 30 degrees, respectively.

Due to the small aperture of conventional endorectal probes, PAT of prostate when conducted in a noninvasive transrectal manner can only be achieved with a limited-viewing angle for signal detection (normally less than 30 degree). Therefore in this study, instead of using a conventional endorectal probe that is commonly used in endoscopic US evaluation of the prostate [31], we have examined the feasibility of PAT for prostate using a phased array that has a larger footprint (28.2-mm long) and enables a comparatively larger view angle for the detection of photoacoustic signals from subsurface lesions (about 60 degree at a depth of 25 mm). This phased array with 128 elements works in a relatively low frequency range of 1-4 MHz that also facilitates more sensitive detection of large-scale, light-absorbing objects such as cancerous lesions in the prostate. Although scanning with limited-viewing angle cannot be avoided for transrectal imaging, a specially designed endorectal probe with a longer footprint could be employed and should contribute to the improvement of image quality and quick acceptance of PAT in the clinic. A specially designed photoacoustic endorectal probe should also enable better receive sensitivity over a broader bandwidth, both of which are essential to achieve satisfactory performance for future clinical management of prostate cancer. Another concern of clinical adaptation of PAT to prostate imaging is the delivery of laser light noninvasively. The illumination of the prostate could be realized via the rectum through an optical fiber array integrated in the rectal probe, similar to the design employed in trans-rectal near-infrared optical tomography of the prostate [14].

#135176 - $15.00 USD Received 15 Sep 2010; revised 1 Oct 2010; accepted 5 Oct 2010; published 7 Oct 2010

In this work, PAT was achieved using a commercial medical US unit without affecting its original imaging functions. This allowed dual-modality imaging of a canine prostate offering both optical and ultrasonic information. The development of PAT for prostate cancer should be accelerated by taking advantage of state-of-the-art commercial US image processing, management and display technologies. For example, PAT of canine prostates in this study was achieved at a fast speed by acquiring data from the 64 parallel ultrasound channels each with commercial-grade receiver sensitivity and noise figures. These and other imaging findings, when derived from a commercially available US system, should be more easily reproduced between laboratories, and introduced more quickly into the clinic. In comparison with PAT, US is a more established imaging modality for prostate cancer. Therefore, interpretation of US images of a prostate specimen may help guide the PAT procedure and interpretation. As an example, the morphological features including the organ boundary and the urethra as presented by the gray-scale US images has helped to identify the accurate location of the lesion visualized by PAT. In the future, tissue acoustic information provided by US, e.g. acoustic attenuation and speed of sound, may also be used to improve the reconstruction of PAT images, which may elevate the accuracy in quantitative imaging of prostate tissue optical properties and hemodynamic parameters.

Acknowledgments

This work was supported in part by the Department of Defense grant number W81XWH-07-1-0231, and National Institute of Health (NIH) grant number R01 AR055179. We thank Larry Mo, Derek DeBusschere and Glen Mclaughlin from Zonare Medical Systems, Inc. for their contributions to the development of imaging system. We also thank Justin Rajian and Zhixing Xie for their help in the experiments.

#135176 - $15.00 USD Received 15 Sep 2010; revised 1 Oct 2010; accepted 5 Oct 2010; published 7 Oct 2010